Received: 17 August 2018 | Revised: 18 October 2018 | Accepted: 8 November 2018

DOI: 10.1111/ejn.14275

RESEARCH REPORT

WILEY EJN European Journal of Neuroscience FENS

Vagus nerve spiking activity associated with locomotion and cortical arousal states in a freely moving rat

Yu Shikano[1*] | **Yuya Nishimura**[1*] | **Toya Okonogi**[1*] | **Yuji Ikegaya**[1,2] | **Takuya Sasaki**[1,3]

[1]Laboratory of Chemical Pharmacology, Graduate School of Pharmaceutical Sciences, The University of Tokyo, Tokyo, Japan

[2]Center for Information and Neural Networks, Suita City, Osaka, Japan

[3]Precursory Research for Embryonic Science and Technology (PRESTO), Japan Science and Technology Agency (JST), Saitama, Japan

Correspondence
Takuya Sasaki, Laboratory of Chemical Pharmacology, Graduate School of Pharmaceutical Sciences, The University of Tokyo, Tokyo, Japan.
Email: tsasaki@mol.f.u-tokyo.ac.jp

Funding information
the Yamada Research Grant; Precursory Research for Embryonic Science and Technology from the Japan Science and Technology Agency, Grant/Award Number: JPMJPR1785; Kaken-hi, ; Exploratory Research for Advanced Technology, Grant/Award Number: JPMJER1801; Nakatomi Foundation; Suzuken Memorial Foundation; Yamada Research Grant

Abstract

The vagus nerve serves as a central pathway for communication between the central and peripheral organs. Despite traditional knowledge of vagus nerve functions, detailed neurophysiological dynamics of the vagus nerve in naïve behavior remain to be understood. In this study, we developed a new method to record spiking patterns from the cervical vagus nerve while simultaneously monitoring central and peripheral organ bioelectrical signals in a freely moving rat. When the rats transiently elevated locomotor activity, the frequency of vagus nerve spikes was correspondingly increased, and this activity was retained for several seconds after the increase in running speed terminated. Spike patterns of the vagus nerve were not robustly associated with which arms the animals entered on an elevated plus maze. During sniffing behavior, vagus nerve spikes were nearly absent. During stopping, the vagus nerve spike patterns differed considerably depending on external contexts and peripheral activity states associated with cortical arousal levels. Stimulation of the vagus nerve altered rat's running speed and cortical arousal states depending on running speed at the instant of stimulation. These observations are a new step for uncovering the physiological dynamics of the vagus nerve modulating the visceral organs such as cardiovascular, respiratory, and gastrointestinal systems.

KEYWORDS

heart rate, local field potential, locomotion, vagus nerve stimulation

1 | INTRODUCTION

The vagus nerve plays a pivotal role in the brain–body communication. The majority of the vagus nerve consists of afferent sensory pathways that transmit ascending information to the nucleus of the solitary tract in the brain from the visceral organs. Especially, previous studies have revealed detailed anatomical pathways innervating from the heart (Hayakawa, Kuwahara-Otani, Maeda, Tanaka, & Seki, 2011), the food intake-related digestive organs (Campos, Wright, Czaja, & Ritter, 2012; Czaja, Ritter, & Burns, 2006), and the lung (Han et al., 2018; Weijs et al., 2015). Furthermore, the afferent vagus nerve has been targeted in studies of interoception, a neurophysiological process by which the brain monitors internal physiological states of the peripheral organs (Garfinkel & Critchley, 2016; Pfeifer et al., 2017), which leads to changes in brain functions, including cognition and emotion. On the other hand, only a small component of the vagus nerve consists of efferent nerves that are part of the parasympathetic nervous system and control functions of the circulatory and digestive

[*]These authors contributed equally to this work.

Edited by Paul Bolam. Reviewed by Sven Kroener and Krzysztof Czaga.

All peer review communications can be found with the online version of the article.

systems (Agostoni, Chinnock, De Daly, & Murray, 1957; Evans & Murray, 1954; Prechtl & Powley, 1990).

Clinically, vagus nerve stimulation (VNS) has been applied to inhibit central nervous system diseases, such as refractory epilepsy (Ben-Menachem et al., 1994; Takaya, Terry, & Naritoku, 1996) and treatment-resistant depression (Nemeroff et al., 2006; Wani, Trevino, Marnell, & Husain, 2013). Consistently, studies using rodents have demonstrated that artificial modulation of vagus nerve activity can alter brain electrical activity (Alexander et al., 2017; Cao et al., 2016; Larsen et al., 2016; Usami et al., 2013), stop seizures (Woodbury & Woodbury, 1990), evoke emotional responses, facilitate learning and decision-making (Alvarez-Dieppa, Griffin, Cavalier, & McIntyre, 2016; Cao et al., 2016; Pena et al., 2014; Suarez et al., 2018), even reduce food intake and body weight (Johannessen et al., 2017), and cardiac hemodynamic effects through activation of the efferent parasympathetic pathway (Yamakawa et al., 2015).

While early studies performed vagus nerve recordings from anesthetized animals (Caravaca et al., 2017; Harreby, Sevcencu, & Struijk, 2011; McCallum et al., 2017; Silverman et al., 2018), recordings from freely moving animals have been limited due to technical difficulties. To address this issue, we developed a novel recording method that can monitor vagus nerve (VN) spikes with a cuff-shaped electrode from a freely moving rat. We hypothesized that a potential role of VN spikes should be to sense various activity patterns of the body such as locomotion and oscillatory peripheral organ activity such as respiration and heartbeat. In addition, VN spikes might be associated with activity states of the central nervous systems. To examine these basic physiological dynamics of the vagus nerve in relation to the central and peripheral organs, we integrated the VN recordings into our recording technique that captures local field potentials (LFPs) from multiple brain regions together with electroencephalogram (ECG), electromyogram (EMG), and breathing (BR) electrical signals (Okada, Igata, Sakaguchi, Sasaki, & Ikegaya, 2016; Sasaki, Nishimura, & Ikegaya, 2017; Shikano, Sasaki, & Ikegaya, 2018). From large-scale electrophysiological datasets, our analyses specifically addressed physiological issues of how VN spike patterns undergo acute changes in relation to (a) locomotor activity, (b) peripheral organ activity such as heartbeats and respiration, and (c) cortical arousal levels in freely moving rats.

2 | MATERIALS AND METHODS

2.1 | Ethical approval

All experiments were performed with the approval of the animal experimental ethics committee at the University of Tokyo (approval number: P29-7) and in accordance with the NIH guidelines for the care and use of animals.

2.2 | Animals

A total of fourteen male Sprague-Dawley rats were purchased from SLC (Shizuoka, Japan). The animals were eight to nine weeks old, weighed 296–400 g, were maintained with free access to water and food, and were maintained under inverted 12-hr light/12-hr dark conditions (light from 8 pm to 8 am). No animals were excluded from our analyses.

2.3 | Preparation of the micro-drive array

An electrode assembly including recording and stimulating electrodes was prepared as described previously (Okada et al., 2016; Sasaki et al., 2017; Shikano, Sasaki, et al., 2018). The electrode assembly was composed of an electrical interface board (EIB) (EIB-36-PTB, Neuralynx, Inc., Bozeman, MT) that consisted of an outer cover and a core body, which were custom-made by 3D printers (UP Plus2, Tiertime, Beijing, China; formlabs Form2, Formlabs, Somerville, MA). The EIB had a sequence of metal holes (channels) for connections with wire electrodes, including two LFP channels, two ECG channels, two EMG channels, two BR channels, two VN channels, and two ground/reference (g/r) channels (Figure 1a). The individual channels were connected to insulated wires (~5 cm), and the opposite ends of these wires were soldered to individual electrodes at the final step of the surgery.

2.4 | Surgery

The animals were anesthetized with 3% isoflurane gas and then maintained with 1-2% isoflurane gas while lying on their backs. Buprenorphine (0.05 mg/kg, s.c.) was given as an analgesic. Veterinary ointment was placed on the rat's eyes to prevent dryness. For all steps of an incision, the skin was sterilized with betadine and 70% ethanol. For each rat, an incision was made in the left neck area from the larynx to the sternum, and the bundle including the VN and the carotid artery were isolated. The left cervical VN was isolated from the surrounding tissue and the left carotid artery. The isolated nerve was enclosed by a custom-made cuff-shaped VN electrode (Unique Medical Co., Ltd., Japan; inner diameter = 0.5–1.0 mm, electrode area = 0.25 mm^2, cathode–anode interval = 1.5–2.0 mm, and total length 4.0 mm) (Figure 1a, VN). The open ends of the VN electrode were extruded from the incision. After implantation of the VN electrode, all rats underwent surgery to implant the ECG, EMG, BR, and LFP electrodes as described previously (Okada et al., 2016; Sasaki et al., 2017; Shikano, Sasaki, et al., 2018). Briefly, two ECG electrodes (stainless-steel wires; AS633, Cooner Wire Company, CA) were attached to the intercostal muscles on both sides of the chest (Figure 1a, ECG), and two EMG electrodes were sutured to the dorsal

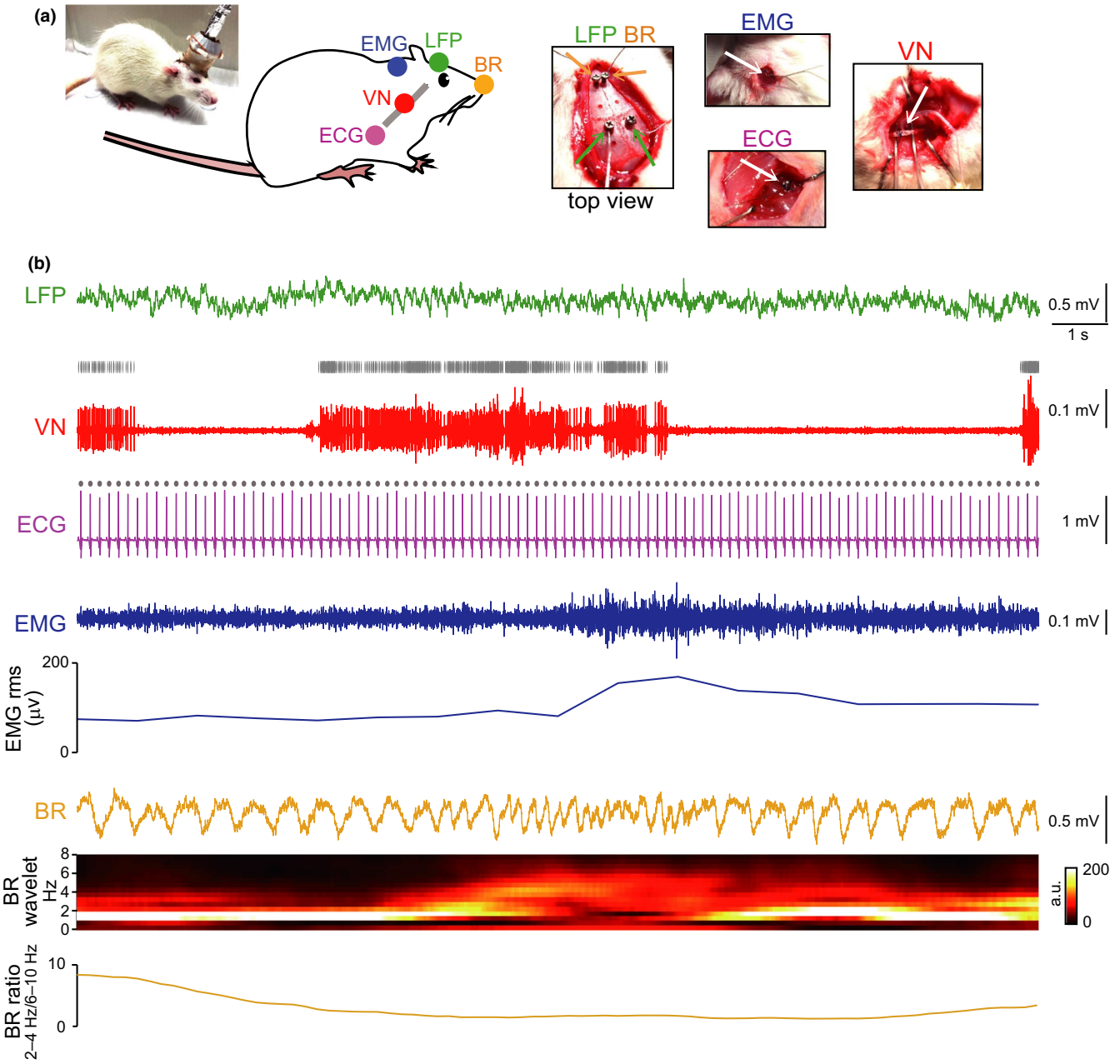

FIGURE 1 Simultaneous recordings of bioelectrical signals from central and peripheral organs including the vagus nerve. (a) (Left) Schematic illustration showing locations of the individual recording electrodes implanted in a rat. (Right) Magnified pictures showing a surgery implanting the tip of each recording electrode onto each tissue (arrows). For VN recording, the left cervical VN was covered with a cuff-shaped VN electrode. All wires protruding from each electrode were connected to the core of an electrode assembly on the animal's head. (b) Example electrical traces simultaneously recorded from a freely moving rat. From top to bottom, cortical LFP signal, VN signal with the extracted spike timing indicated by gray dots above, ECG signal with the R-peak timing indicated by gray dots above, EMG signal with the magnitude (root-mean-square amplitude) shown below, and BR signal with the wavelet power spectrum and the BR ratio of 2–4 Hz power to 6–10 Hz power shown below. [Colour figure can be viewed at wileyonlinelibrary.com]

neck area (Figure 1a, EMG). For implantation of the LFP electrodes in the motor cortex, a midline incision was made above the skull, and circular craniotomies with a diameter of 0.9 mm were made with a high-speed drill (SD-102, Narishige, Tokyo, Japan) at coordinates of 0.3 mm posterior and 1.9 mm bilateral to the bregma. Stainless-steel screw-shaped LFP electrodes were implanted on the surface of the craniotomies (Figure 1a, LFP). For implantation of the BR electrodes on the olfactory bulb, circular craniotomies with a diameter of 0.9 mm were made at coordinates of 10.0 mm anterior and 0.2–0.5 mm bilateral to the bregma. Stainless-steel screw-shaped BR electrodes were implanted on the surface of the craniotomies (Figure 1a, BR). In addition, stainless-steel screws were implanted on the surface of the cerebellum (9.6 mm anterior and 0.8–1.0 mm bilateral to the bregma) as ground/reference (g/r) electrodes. Finally, the open edges

of the ECG, EMG, VN, BR, LFP, and g/r electrodes were soldered to the open edges of the insulated wires protruding from the corresponding channels on the EIB. All the wires and the electrode assembly were secured to the skull using dental cement. For the vagus nerve stimulation (VNS) experiments, a custom-made stimulation electrode that included a bioflex wire (FEP Hookup Wire Stranded Stainless-Steel AS 633, Cooner Wire Company, Chatsworth, CA) and a silicon tube (~7.0 mm) was attached to the VN. The open ends of the VNS electrodes were soldered to a socket attached to an electrode assembly as described previously (Shikano, Ikegaya, & Sasaki, 2018). After fixing all the electrodes on the animals' heads, the animals were recovered from anesthesia. Following surgery, each animal was single housed in a transparent Plexiglas cage with free access to water and food.

2.5 | Electrophysiological recordings

Electrophysiological recordings commenced more than four days after the surgery. For recording of the electrophysiological signals, the EIB of the electrode assembly was connected to a digital headstage Cereplex M (Blackrock Microsystems), and the digitized signals were transferred to a data acquisition system, Cereplex Direct (Blackrock Microsystems). LFP, ECG, EMG, and BR signals were recorded at a sampling rate of 2 kHz, and VN signals were recorded at a sampling rate of 10–30 kHz. For the VNS experiments, a socket was connected to an electrical stimulator (SEN-3301, Nihon Kohden, Tokyo, Japan) (Shikano, Ikegaya, et al., 2018), and trains of 60 electrical pulses (1 mA) at a frequency of 20 Hz with a pulse duration of 1.5–3.0 ms were applied to the VN every 30 s. An analog input system running from the electric stimulator to the data acquisition system via VNC connectors specified the timings of the electrical pulses during recording.

2.6 | Behavioral tests

All behavioral tests occurred in the rats' dark phase from 9 am to 5 pm. The animals were not handled at all before starting the following procedures. One day before behavioral tests, the animals were first located in a transparent rest box (22×38 cm^2) with a wall height of 20 cm at least once for up to 30 min. The rest box was placed at least 2 m distant from these recording setups and a barrier wall was placed, so that the rats in the rest box could not directly see the open field and the elevated plus maze. On a recording day, the rats were habituated in the same rest box for 2 hr and electrophysiological recording first started in the rest box. Throughout these habituation periods one day before and on the recording day, the rats were habituated to tethering by connecting to the headstage.

For recordings in a novel open field, the rat was then placed in an open field (75×75 cm^2) with a wall height of 50 cm and allowed to move freely throughout the field for 10 min. The floor was illuminated with an overhead light, which produced light intensities of 25 lux in the field.

For recordings in a novel elevated plus maze, the rat was then placed on the central square facing the open arm and allowed to freely explore the maze apparatus for 10 min. The elevated plus maze was made of ABS resin and consisted of a central square (10×10 cm^2) and four arms (50 cm long $\times$ 10 cm wide, two open arms with no railing and two closed arms enclosed by a transverse wall 40 cm in height). The maze was elevated 88.5 cm from the floor and illuminated with four 32-W fluorescent overhead lights, which produced light intensities of 480 lux and 40 lux in the open and closed arms, respectively.

For all recordings, a LED reflection tape (1×1 cm^2) was attached to the outer cover of the electrode assembly, and the position of the LED signal was tracked at 15 Hz using an infrared video camera attached to the ceiling, which was sampled by a laptop computer. Rat's moment-to-moment positions were automatically detected from the LED reflection tape by setting a threshold of light intensity.

2.7 | Data analysis

The signals that included apparent electrical noise due to physical striking of the animal's head to the walls were manually removed. For the VN signals, a spike unit was detected when the amplitude of a negative deflection of the extracellularly recorded signals exceeded a threshold of 7–20 μV, which corresponded to five standard deviations from the baseline of the VN signals recorded during quiescent periods in individual animals. Spike units detected within a 10-ms bin were regarded as a single spike. Cortical LFP traces were convolved by a Morlet's wavelet family. ECG signals were bandpass filtered at 20–200 Hz, and beat-to-beat intervals (R-R intervals) were calculated from the timestamp of the R-wave peak. Instantaneous heart rates were computed by averaging the R-R intervals in each 1-s bin. EMG traces were high-pass filtered at 100 Hz, and root-mean-square (RMS) values were calculated from the filtered EMG traces with a bin size of 1 s, which have been used to define the animal's movement and arousal state (Hayashi et al., 2015; Oishi et al., 2016). BR signals were convolved by a Morlet's wavelet family and the ratio of 6–10 Hz power to 2–4 Hz power was computed as the BR ratio (Okonogi, Nakayama, Sasaki, & Ikegaya, 2018), which was used to detect sniffing, a typical exploratory behavior.

The animals' peripheral activity states were classified in each 1-s frame bin as follows (Figure 3a): (a) "movement" periods were defined when running speed was more than 5 cm/s; (b) without movement periods, "sniffing" periods were defined when BR ratios were <2, (c) without movement and sniffing periods, "active stop" periods were defined

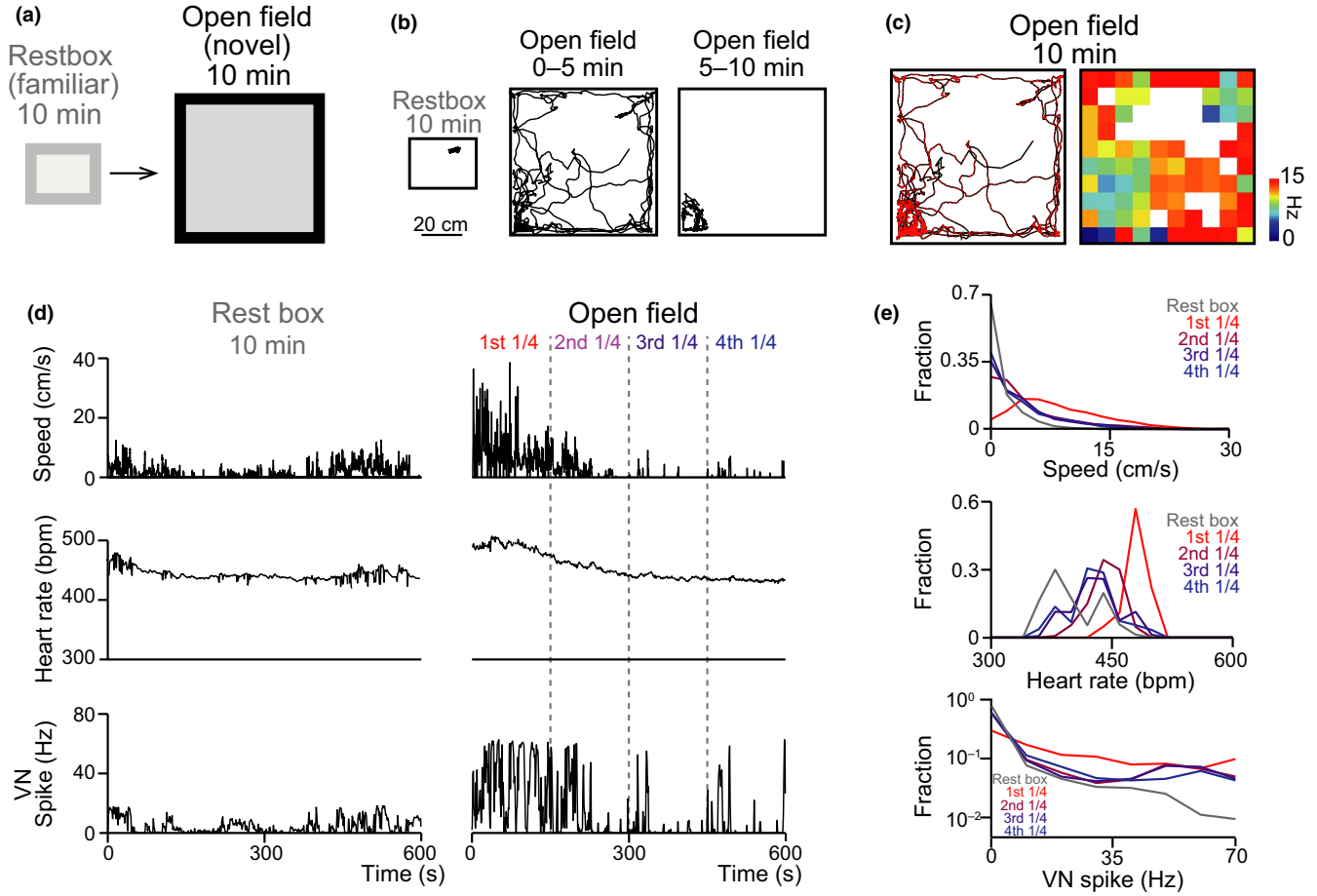

FIGURE 2 VN spike patterns in a novel open field. (a) On a recording day, a rat was sequentially placed in a familiar rest box and in a novel open field for 10 min each. (b) Representative trajectories of a rat in the rest box and in the novel open field. The trajectory in the open field for the first and second 5-min sessions is shown separately. (c) (Left) Positions of VN spikes represented as red dots superimposed on position trajectories (gray lines) observed from the same rat in the 10-min period in the open field. (Right) The corresponding color-coded spike rate map (blue, 0 Hz; red, 15 Hz). (d) Changes in instantaneous running speed, VN spike rates, and heart rates recorded from the rat in the rest box and open field. The 10-min periods were divided into four periods. (e) Distribution of running speed, heart rates, and VN spike rates in each 1/4 period. Each point was computed in each 1-s bin ($n = 5$ animals). [Colour figure can be viewed at wileyonlinelibrary.com]

when instantaneous heart rates exceeded a certain threshold, heart $\text{rate}_{\text{criterion}}$, and the RMS of EMG signals exceeded a certain threshold, $\text{RMS}_{\text{criterion}}$. Here, heart $\text{rate}_{\text{criterion}}$ is the minimum heart rate plus 30 bpm (408 ± 10.7 bpm, ranging from 390 bpm to 450 bpm, $n = 5$ animals), and $\text{RMS}_{\text{criterion}}$ is twice the average of the bottom 20% RMS values observed within a 10-min session in the rest box. These criteria were set as the lowest limits of heart rates and EMG amplitudes to distinguish high and low peripheral activity states. The other periods that were not classified into the above three states were classified as "silent stop", which was considered as stabilized peripheral states at low activity levels, termed as low peripheral (LP) activity states reported in our previous study (Okonogi et al., 2018).

All analyses were performed in MATLAB (MathWorks). In Figures 2, 3 and 5, a difference between a pair of distributions was assessed by a Kolmogorov–Smirnov test. Multiple group comparisons were performed by individual tests followed by posthoc Bonferroni corrections. In Figure 2, correlational changes between running speed, heart rates, and VN spike rates were assessed by computing Pearson's correlation coefficients. In Figure 4f, changes in theta/delta ratios across multiple behavioral patterns were assessed using a repeated-measures ANOVA. In Figure 7, running speed or LFP power before and after VNS were compared by paired t test. The null hypothesis was rejected at the $p < 0.05$ level unless otherwise specified. All data are presented as the mean ± standard error of the mean (SEM).

3 | RESULTS

3.1 | Recordings of vagus nerve spikes with cortical and peripheral bioelectrical signals

Recordings of VN signals were performed by wrapping the cervical VN with a cuff-shaped electrode with the electrode

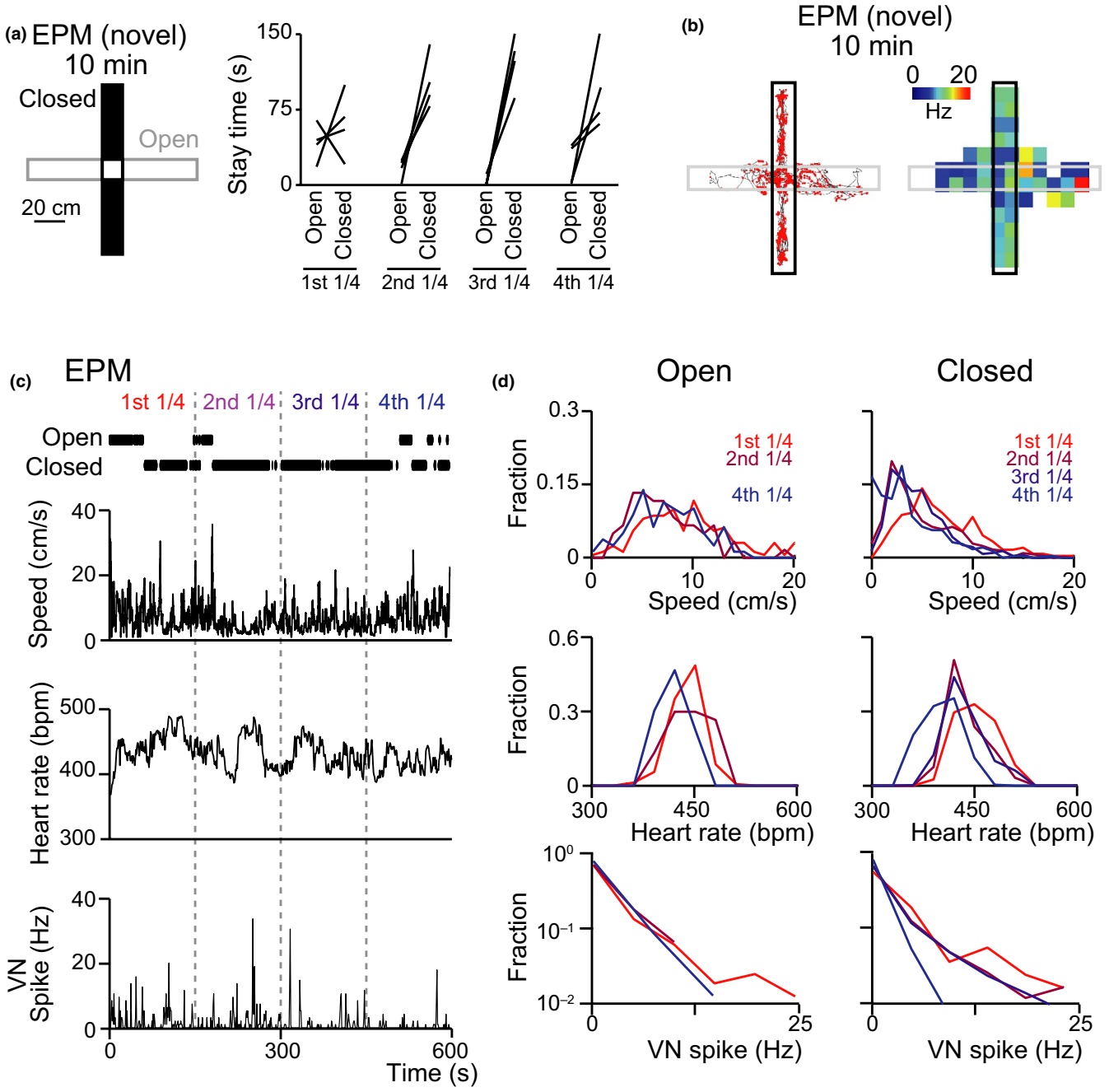

FIGURE 3 VN spike patterns in a novel EPM. (a) (Left) An overview of the EPM. A rat was subjected to a novel EPM for 10 min. (Right) Duration of time spent in open and closed arms in each 1/4 period (150 s) of the 10-min EPM test. Each line shows each animal ($n = 4$ animals). (b) (Left) Positions of VN spikes represented as red dots superimposed on position trajectories observed from a rat in the 10-min period in the EPM test. (Right) The corresponding color-coded spike rate map (blue, 0 Hz; red, 20 Hz). (c) Arm types where the animal was located in the 10-min EPM test are represented as black ticks in the top panel. Lower panels show changes in instantaneous running speed, VN spike rates, and heart rates. (d) Distribution of running speed, heart rates, and VN spike rates in each 1/4 period of the 10-min EPM test. Each point was computed in each 1-s bin ($n = 4$ animals). [Colour figure can be viewed at wileyonlinelibrary.com]

contact sites attached to the inside walls of the cylindrical tube (Figure 1a). This recording method reduced background noise and increased the signal to noise ratio (Caravaca et al., 2017; Sahin & Durand, 1998; Silverman et al., 2018). The open edge of the cuff-shaped electrode was connected to an electrical board on an electrode assembly attached to the animal's head (Shikano, Sasaki, et al., 2018). This configuration enabled the recording of VN spikes with cortical LFP, ECG, EMG, and BR signals, from a freely moving rat (Figure 1). We ruled out the possibility that the VN signals were a mere electrical replication arising from other peripheral signals based on the following observations. First,

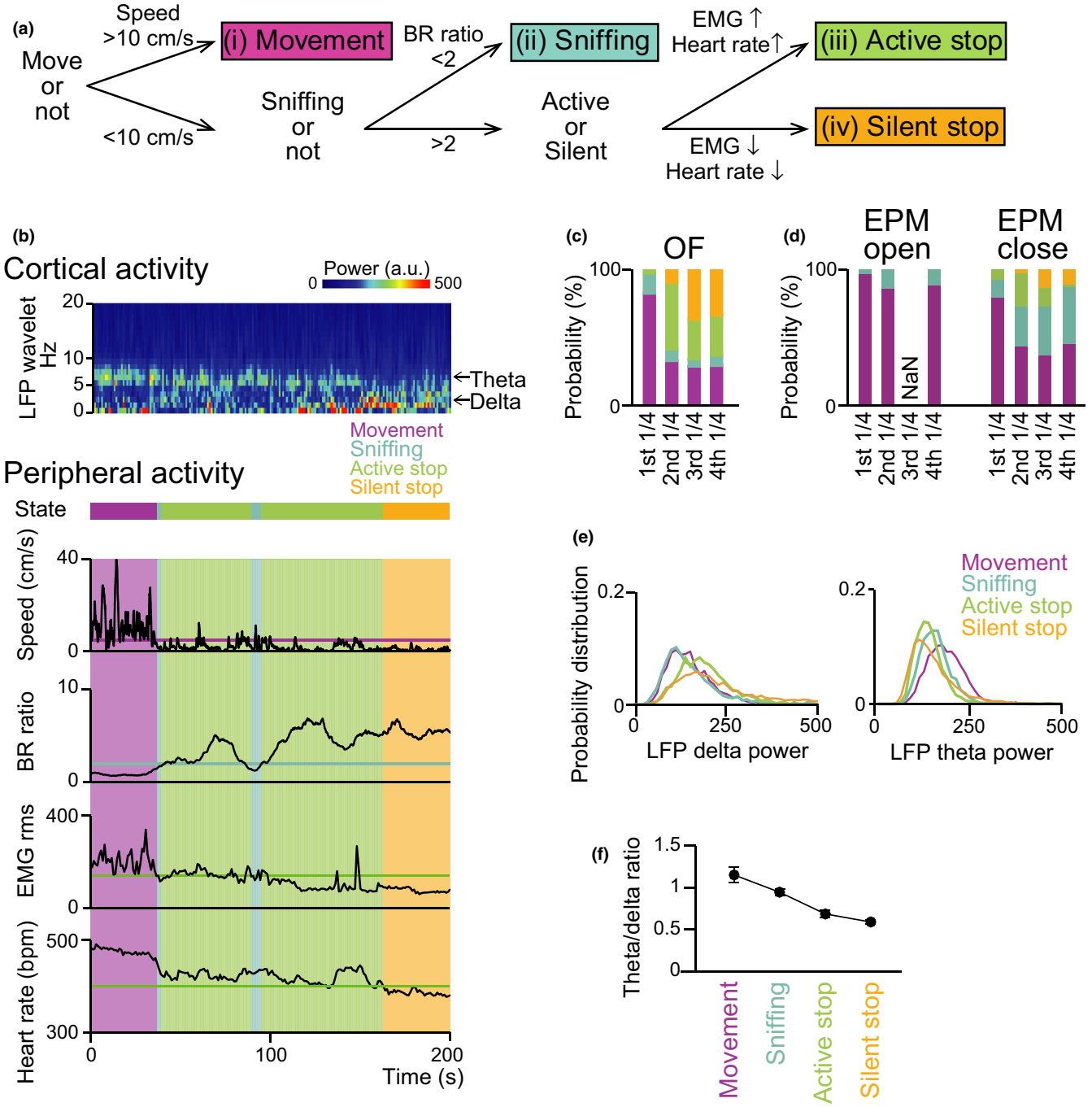

FIGURE 4 Animal's peripheral activity states and cortical arousal levels. (a) Classification of an animal's peripheral activity states: (i) "movement" periods were extracted based on running speed, (ii) "sniffing" periods were extracted based on BR ratios, (iii) "active stop", and (iv) "silent stop" periods were defined based on EMG and heart rates. (b) Representative change patterns of peripheral states in the open field. Peripheral states were defined by running speed, BR ratio, EMG rms, and heart rates (four bottom panels), and are color-coded. The cyan line defines a BR ratio of 2 to detect sniffing. The green lines define the threshold of EMG amplitude and heart rate used to distinguish between the active and silent stop periods. The top panel shows the power spectrum constructed from a LFP signal at the corresponding period. Delta and theta frequency bands are indicated by arrows. (c) Probability distribution of duration of individual behavioral patterns in the first to fourth 1/4 periods of the entire 10-min period in the open field. (d) Same as C but for the EPM test. Data are separately shown for open and closed arms. (e) Probability distribution of delta and theta power in each peripheral activity state. Data were obtained from individual 0.5-s bins from 5 animals in the rest box and open field (movement, $n = 2970$ bins; sniffing, 1736 bins; active stop, 2664 bins; silent 4630 bins). (f) The averaged ratio of delta power to theta power. $F_{3,34} = 20.67$, $p = 8.3 \times 10^{-8}$. [Colour figure can be viewed at wileyonlinelibrary.com]

heartbeats with transient positive deflections (R-peaks) in the ECG signals were not reflected in the VN signals (Figure 1b, VN and ECG). Second, respiratory rate changes in the BR signals, especially including sniffing behavior, were not reflected in the VN signals (Figure 1b, VN and BR). Third, movement-induced transient deflections, represented by increases in the RMS of the dorsal neck muscle EMG signals, were not reflected in the VN signals (Figure 1b, VN and EMG).

3.2 | VN spike patterns in a familiar box and a novel open field

The animals were sequentially placed into two different environments, familiar (rest box) and novel recording boxes (open field). In the following experiments (Figures 2 and 4–6), five animals were recorded in one 10-min rest box and one 10-min open field sessions. All recorded animals were used for analyses. After the animals were habituated to the rest box for at least 2 hr, electrophysiological data collection started in the rest box (Figure 2a). In the rest box, the animals were familiar with the environment and remained nearly immobile throughout a 10-min recording period (Figure 2b), with their running speed <5 cm/s for 92.6% of the recording periods (Figure 2d,e; $n = 5$ animals), and their heart rates were stabilized at an average rate of 402.6 ± 14.1 bpm and an average heart rate variability of 13.9 ± 2.7 bpm (Figure 2b–e). In this condition, instantaneous VN spike rates computed in 1-s bins were 0 Hz in 63.5% of the recording periods. When the animals briefly moved in the rest box, VN spike rates were transiently increased to an average spike rate of 18.1 ± 0.6 Hz within the active 1-s bins.

After the 10-min recording session in the rest box, the animals were placed into a novel open field (open field) and allowed to move freely throughout the field for 10 min (Figure 2a,b). As shown in Figure 2d, animal's running speed became prominently higher in the field especially in the first 2-3 min period. To examine such temporal changes, we analyzed datasets with dividing the 10-min period into four periods (from first to fourth 1/4 period). The distribution of animal's running speed shown in Figure 2e demonstrates that running speeds were significantly highest in the first 1/4 period (first vs. second, $D_{max} = 0.40$, $p < 10^{-100}$; first vs. third, $D_{max} = 0.46$, $p < 10^{-100}$; first vs. fourth, $D_{max} = 0.43$, $p < 10^{-100}$; Kolmogorov–Smirnov tests followed by posthoc Bonferroni corrections). This result is presumably because the rats were highly motivated when they were first placed in the novel environment. Consistently, heart rates in the first 5-min period were 480.3 ± 7.0 bpm and significantly higher than those in any other periods (first vs. second, $D_{max} = 0.81$, $p < 10^{-100}$; first vs. third, $D_{max} = 0.80$, $p < 10^{-100}$; first vs. fourth, $D_{max} = 0.74$, $p < 10^{-100}$; Kolmogorov–Smirnov tests followed by posthoc Bonferroni corrections), which then decreased to averages of 428.5 ± 14.7 bpm in the fourth 5-min period. Instantaneous running speed and heart rates were positively correlated, with an average Pearson's correlation coefficient of 0.63 ± 0.05 ($p < 0.001$ in all five animals tested; ranging from 0.50 to 0.74), demonstrating that the animal's running speed is well reflected by changes in heart rate. In this novel open field, average VN spike rates in the first 1/4 period considerably increased to 21.1 ± 3.8 Hz (first vs. second, $D_{max} = 0.30$, $p = 3.9 \times 10^{-29}$; first vs. third, $D_{max} = 0.35$, $p = 3.7 \times 10^{-41}$; first vs. fourth, $D_{max} = 0.34$, $p = 2.1 \times 10^{-38}$; Kolmogorov–Smirnov tests followed by posthoc Bonferroni corrections) (Figure 2e). In the second to the fourth 1/4 period, consistent with the decreases in running speed and heart rates, VN spike rates were significantly lowered (comparison between first 1/4 period and all other periods, $p < 10^{-10}$, Kolmogorov–Smirnov tests followed by posthoc Bonferroni corrections). The VN spikes were not localized within a particular area, showing no place-specific spikes of the VN (Figure 2c). Changes in VN spike rates were partly correlated with changes in running speed and heart rates, with correlation coefficients of 0.21 ± 0.16 (ranging from −0.38 to 0.61) and 0.33 ± 0.11 (ranging from 0.00 to 0.65), respectively, which were prominently lower than the correlation coefficients computed for the relationship between heart rates and running speed (0.63 ± 0.05).

3.3 | VN spike patterns in a novel elevated plus maze

We next examined VN spike patterns in a 10-min elevated plus maze (EPM) test (Figure 3a). Here, four rats that were different from the five rats used for the open field test were tested. During the first 1/4 period of the EPM test, stay time in open and closed arms was not significantly different (Figure 3a; $n = 4$ rats; $t_3 = 0.74$, $p > 0.99$, paired t test with Bonferroni correction). During the next three 1/4 periods (from 2.5 to 10 min), stay time in closed arms was longer than that in open arms, although they were not significant in some periods (Figure 3a; second, $t_3 = 4.72$, $p = 0.054$; third, $t_3 = 7.58$, $p = 0.015$; fourth, $t_3 = 1.53$, $p = 0.67$, paired t test followed by Bonferroni correction). Analyses for cumulative distributions demonstrated that running speed in both open and closed arms in the first 1/4 period was significantly higher than those in the other periods (Figure 3d, top; open, first vs. second, $D_{max} = 0.28$, $p = 0.0032$; first vs. fourth, $D_{max} = 0.22$, $p = 0.018$; closed, first vs. second, $D_{max} = 0.31$, $p = 4.2 \times 10^{-13}$; first vs. third, $D_{max} = 0.30$, $p = 7.5 \times 10^{-13}$; first vs. fourth, $D_{max} = 0.44$, $p = 1.6 \times 10^{-22}$, Kolmogorov–Smirnov tests followed by Bonferroni correction). As the three (out of four rats tested) did not enter into open arms during the third 1/4 period, this period was excluded from all analyses. Furthermore, running speed in open arms was significantly higher than that in closed arms in all periods

(first, $D_{max} = 0.26$, $p = 9.0 \times 10^{-6}$; second, $D_{max} = 0.40$, $p = 2.2 \times 10^{-7}$; fourth, $D_{max} = 0.49$, $p = 3.1 \times 10^{-13}$, Kolmogorov–Smirnov tests followed by Bonferroni correction). Overall, these results suggest that the animals first actively moved both in open and closed arms and then became silent preferentially in the closed arms. Similar to these running speed changes, heart rates were highest in the first 1/4 period in both arms (Figure 3d, middle; open, first vs. second, $D_{max} = 0.25$, $p = 0.018$; first vs. fourth, $D_{max} = 0.47$, $p = 8.6 \times 10^{-11}$; closed, first vs. second, $D_{max} = 0.29$, $p = 4.8 \times 10^{-11}$; first vs. third, $D_{max} = 0.29$, $p = 1.5 \times 10^{-11}$; first vs. fourth, $D_{max} = 0.62$, $p = 1.1 \times 10^{-43}$, Kolmogorov–Smirnov tests followed by Bonferroni correction) and significantly different between open and closed arms during individual 1/4 periods (first, $D_{max} = 0.26$, $p = 1.5 \times 10^{-5}$; second, $D_{max} = 0.27$, $p = 2.8 \times 10^{-3}$; fourth, $D_{max} = 0.40$, $p = 1.1 \times 10^{-8}$, Kolmogorov–Smirnov tests followed by Bonferroni correction). In these conditions, VN spike patterns were not localized within a particular area of the maze, showing no place-specific spikes of the VN (Figure 3b). Notably, VN spike patterns were somewhat different from the change patterns of running speed and heart rates (Figure 3d, bottom). First, VN spike rates in open arms were not significantly different across all periods (first vs. second, $D_{max} = 0.10$, $p > 0.99$; second vs. fourth, $D_{max} = 0.10$, $p > 0.99$; first vs. fourth, $D_{max} = 0.11$, $p > 0.99$), whereas VN spike rates in closed arms were significantly highest in the first 1/4 period, compared with the other periods (first vs. second, $D_{max} = 0.15$, $p = 0.0039$; first vs. third, $D_{max} = 0.15$, $p = 0.0057$; first vs. fourth, $D_{max} = 0.40$, $p = 1.2 \times 10^{-18}$). Second, VN spikes were significantly higher in open arms, compared with closed arms, only in the first 1/4 period but not in the second and fourth periods (first, $D_{max} = 0.17$, $p = 0.024$; second, $D_{max} = 0.08$, $p > 0.99$; fourth, $D_{max} = 0.18$, $p = 0.078$, Kolmogorov–Smirnov tests followed by Bonferroni correction). Taken together, these results demonstrate that, first, VN spike rates pronouncedly increased immediately after rats are placed in a novel open environment, corresponding with increased running speed and heart rates, suggesting that these VN spike patterns may be partly explained by novelty and/or novelty-induced elevated locomotion. Second, VN spike patterns did not tightly encode whether rats are located at open or closed environments. Assuming that open and closed arms in an EPM represent differences in animal's anxiety levels, our results suggest that VN spikes are not simply explained by anxiety.

3.4 | VN spikes are associated with peripheral activity states

VN spike patterns were further examined on a seconds time scale. First, according to instantaneous running speed, BR ratio, heart rate, and EMG amplitude, peripheral activity patterns were classified into four states for each 1-s bin: (a) movement, (b) sniffing, (c) active stop, and (d) silent stop (Figure 4a; for more detail, see Materials and Methods). Here, active stop periods were considered as periods in which the running speed was <5 cm/s, but peripheral activity levels were high, whereas silent stop periods were considered periods in which peripheral organ activity was stabilized at low levels, as in our previous study (Okonogi et al., 2018). Figure 4b shows an example of the classification of peripheral activity states with the corresponding cortical LFP signals. Overall, both in the open field and EPM test, as the time proceeded, the proportion of movement periods decreased whereas those of active and silent stop periods tended to increase (Figure 4c,d). LFP signals are composed of collective oscillatory activity, including a large number of neuronal spikes and neurotransmission, and the power of LFP signals at individual frequency bands represents the global activity states of the brain. The delta (1–4 Hz) power is typically increased during rest/sleep periods, whereas theta (6–10 Hz) power is increased when animals are actively moving and engaging in attention-seeking behavior. These power changes are considered as a potential neural substrate for information processing (Buzsaki, 2006). As peripheral activity states shifted from movement, sniffing, active stop, to silent stop, cortical LFP delta power and theta power were increased and decreased, respectively (Figure 4e). This change leads to a pronounced reduction in the theta/delta ratio (Figure 4f; comparison across peripheral activity state, $F_{3,34} = 20.67$, $p = 8.3 \times 10^{-8}$, repeated-measures ANOVA), a neurophysiological marker to estimate the animal's arousal levels. The results confirm that arousal levels estimated from cortical signals were well matched with the order of these peripheral states (from movement, sniffing, active stop, to silent stop).

We then analyzed how VN spike patterns were altered in conjunction with the peripheral activity states. Four examples of changes in VN spike rates are shown in Figure 5a. Exp 1 and Exp 2 represent typical periods in which the overall peripheral states gradually shifted from movement to silent stop periods in the open field, showing that the VN spike rates were decreased as the peripheral states changed. Exp 3 represents a rare case in which peripheral states repeatedly transited between movement and active stop periods in the open field, showing that VN spike rates were increased during the active stop periods compared with those during the movement periods. Exp 4 represents a typical period in which most of periods were classified into silent stop periods with occasional sniffing behavior in the rest box, showing that VN spikes were considerably lowered throughout the recording period. Data from all periods in each condition were analyzed and are summarized in Figure 5b,c. Statistical analyses revealed that VN spike rates in the movement periods were significantly higher than those in any other period in both environments (rest box: movement vs. sniffing,

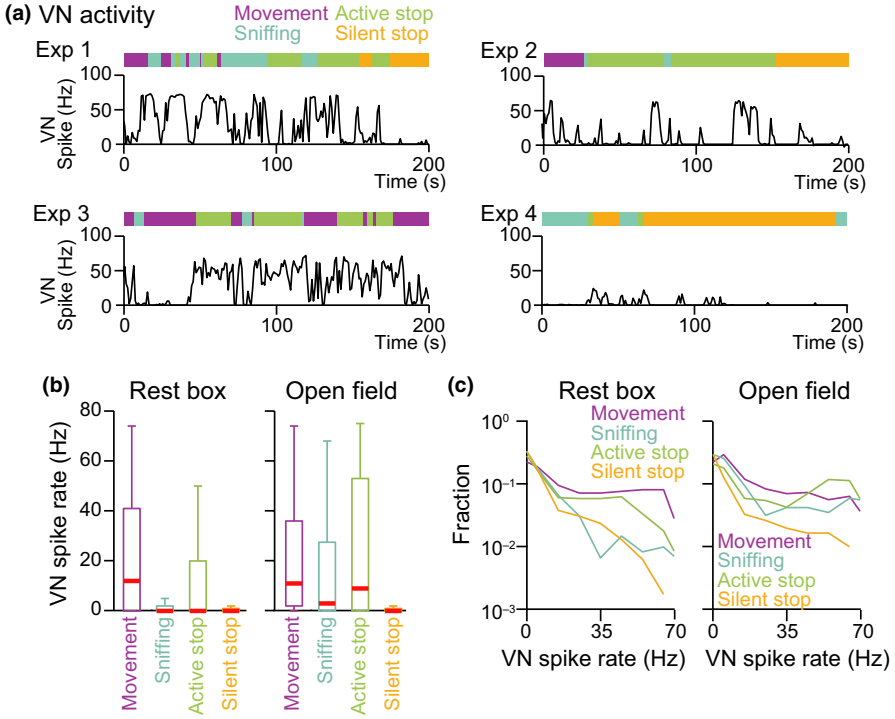

FIGURE 5 VN spike patterns and peripheral activity states. (a) Four examples showing changes in VN spike rates and peripheral activity states, which are color-coded similar to Figure 3a. (b) Box plots of VN spike rates with the median indicated by the red bar ($n = 5$ animals). In the rest box, the median was 0 during sniffing, active stop, and silent stop periods. In the open field, the median was 0 during silent stop periods. (c) Distribution of VN spike rates in each 1-s bin. Data were obtained from five animals in the rest box open field (rest box, movement, $n = 199$ bins; sniffing, 592 bins; active stop, 488 bins; silent 1,721 bins; open field, movement, $n = 1{,}286$ bins; sniffing, 276 bins; active stop, 844 bins; silent 594 bins). [Colour figure can be viewed at wileyonlinelibrary.com]

$D_{max} = 0.43$, $p = 3.2 \times 10^{-24}$; movement vs. active stop, $D_{max} = 0.28$, $p = 1.1 \times 10^{-9}$; movement vs. silent stop, $D_{max} = 0.44$, $p = 3.7 \times 10^{-30}$; open field: movement vs. sniffing, $D_{max} = 0.43$, $p = 3.2 \times 10^{-24}$; movement vs. active stop, $D_{max} = 0.13$, $p = 8.4 \times 10^{-8}$; movement vs. silent stop, $D_{max} = 0.56$, $p = 5.5 \times 10^{-113}$; Kolmogorov–Smirnov test with Bonferroni correction), confirming that VN spikes increased with increases in the animal's locomotor activity. In the open field, the VN spike rates during the sniffing periods were lower than those during the movement and active stop periods (rest box: sniffing vs. active stop, $D_{max} = 0.18$, $p = 5.4 \times 10^{-8}$; open field: sniffing vs. active stop, $D_{max} = 0.17$, $p = 2.3 \times 10^{-5}$; Kolmogorov–Smirnov test), showing that VN spike increases were not apparent during sniffing behavior. During active stop periods, the VN spike rates were higher than those during sniffing and silent stop and differed considerably between the two recording boxes. VN spike rates during active stop periods in the rest box were significantly lower than those in the open field (rest box vs. open field, $D_{max} = 0.25$, $p = 3.0 \times 10^{-17}$; Kolmogorov–Smirnov test). Taken together, these results demonstrate that VN spike patterns are not a simple reflection of shifts in peripheral activity states and cortical arousal levels and depend on the external contexts.

3.5 | Vagus nerve spikes follow running behavior

To further examine the detailed temporal relationship between locomotor behavior and VN spikes on a moment-by-moment basis, instantaneous running speed and VN spike rates were plotted in each 1-s bin and are shown in Figure 6a. A speed increase event was detected when a local maximum of a running speed change exceeded >10 cm/s. Temporal changes in VN spike rates were then aligned to the onset and the peak timing of each event (Figure 6a, right two panels). Averaged data from all events are shown in Figure 6b,c ($n = 65$ and 87 events from five animals, respectively). Figure 6b shows that both VN spike rates and running speed started to increase at the same time, demonstrating that VN spikes are time-locked to the onset of running speed increases. On the other hand, Figure 6c shows that VN spike rate increases were retained at maximum levels 2–5 s after the running speed reached its peak, showing that the decay of VN spikes was delayed a few seconds relative to the decay of running speed. This idea was further confirmed by computing the time interval (i.e., latency) between a running speed peak and the corresponding VN spike rate peak (Figure 6d). Overall, 72.2% of the time intervals were more than 0 s, and the average time interval was 1.5 ± 0.3 s. Taken together, these results demonstrate that VN spike rates are increased immediately following running speed increases, but the return of VN spike rates to baseline after reaching the maximum speed takes a few seconds after running speed starts to decrease.

3.6 | Vagus nerve stimulation alters running speed and cortical activity states

Finally, we examined how transient increases in VN activity evoked by VNS affect running behavior and cortical activity states. The experimental protocols for combining electrophysiological recordings with VNS were similar to

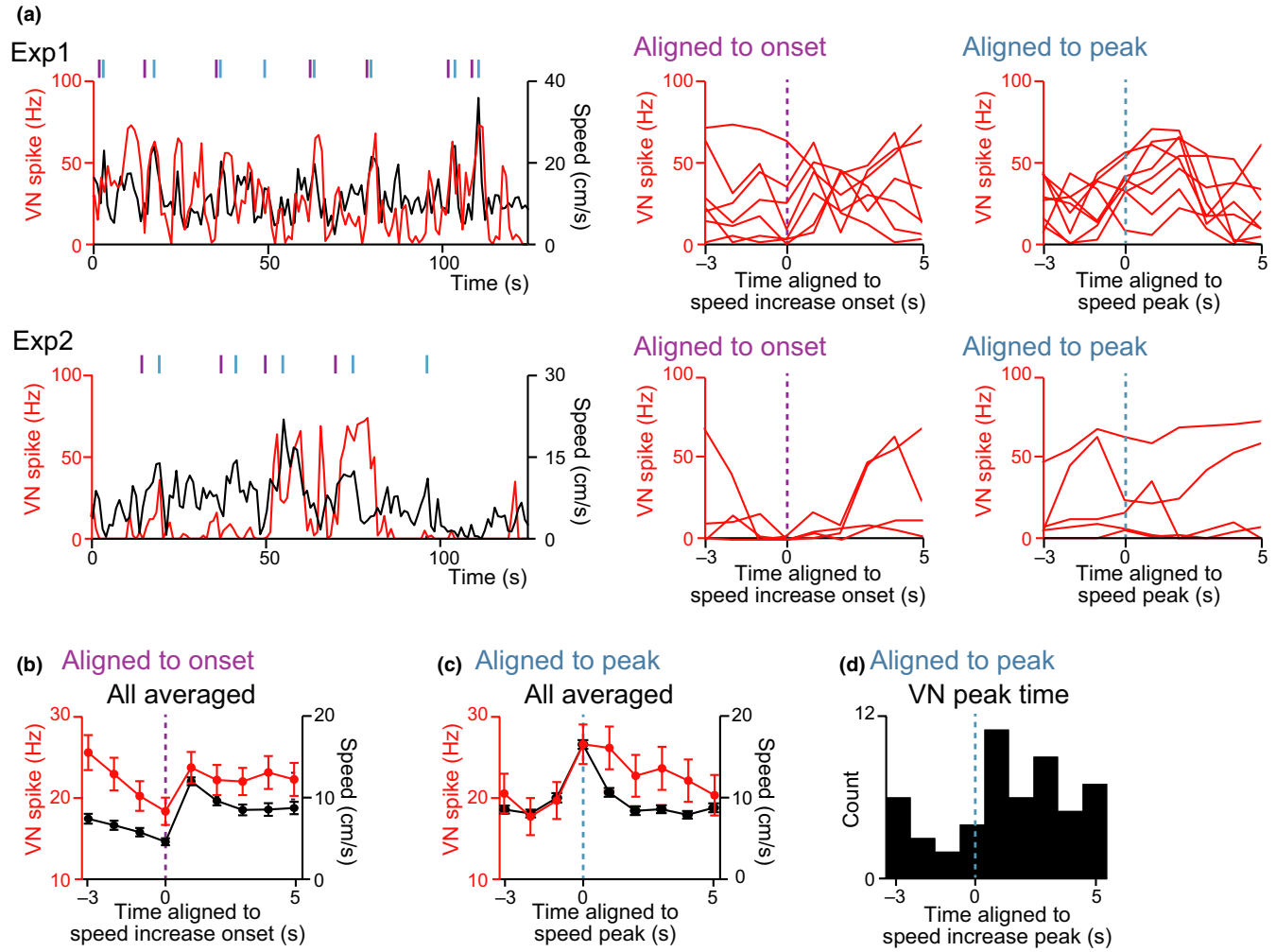

FIGURE 6 Temporal relationship between VN spike rates and running speed. (a) (Left) Two examples showing changes in an animal's running speed (black) and VN spike rates (red). A speed increase event was defined when a running speed peak exceeded more than 10 cm/s. The onset and the peak time of each event are indicated by the purple and cyan lines above, respectively. (Right two panels) The VN spike rate changes were aligned to the onset (purple) and the peak time (cyan) of each event corresponding to the left panels. (b) Averaged VN spike rate changes aligned to the onset of individual speed increase events computed from all rats ($n = 65$ events from five animals). (c) Same as in B but aligned to the peak time of the individual speed increase events ($n = 87$ events from five animals). (d) Distribution of the latency of VN spike rate peaks relative to running speed peaks in individual speed increase events. Data in which VN spike rate peaks were more than 20 Hz were selectively included in this analysis. [Colour figure can be viewed at wileyonlinelibrary.com]

those published in our previous study (Shikano, Ikegaya, et al., 2018). Our previous study confirmed that cortical filtered LFP signals below 150 Hz, which included delta and theta oscillations, were not contaminated with VNS-derived electrical artifacts (Shikano, Ikegaya, et al., 2018). Figure 7a shows representative data of a cortical LFP power spectrum and running speed in response to 60 pulses of VNS (1 mA) at a frequency of 20 Hz with a pulse duration of 1.5–3.0 ms (that is, a total of 3 s from the first to last stimulation pulses, as indicated by the black lines above), applied every 30 s. The effects of VNS were analyzed separately when an instantaneous running speed at VNS was >5 cm/s and <2 cm/s, which were considered as the high and low running speed, respectively. At the two different running speeds, VNS-triggered averages of the temporal changes in running speed and the cortical delta and theta power were plotted (Figure 7b,c). The effects of VNS on running speed differed depending on the instantaneous running speed (Figure 7b). VNS applied at the high running speed significantly decreased the running speed ($t_{36} = 2.35$, $p = 0.025$, paired t test, 3-s periods before vs. during VNS), whereas VNS applied at low running speed evoked a transient increase in the running speed ($t_{102} = 10.12$, $p = 4.3 \times 10^{-17}$). Consistently, VNS altered cortical delta and theta power depending on running speed (Figure 7c). VNS at high running speed increased and decreased cortical delta and theta power, respectively (delta: $t_{77} = 2.14$, $p = 0.035$; theta: $t_{77} = 5.27$, $p = 1.2 \times 10^{-6}$, paired t test, 3-s periods before vs. during VNS), whereas VNS at low running speed

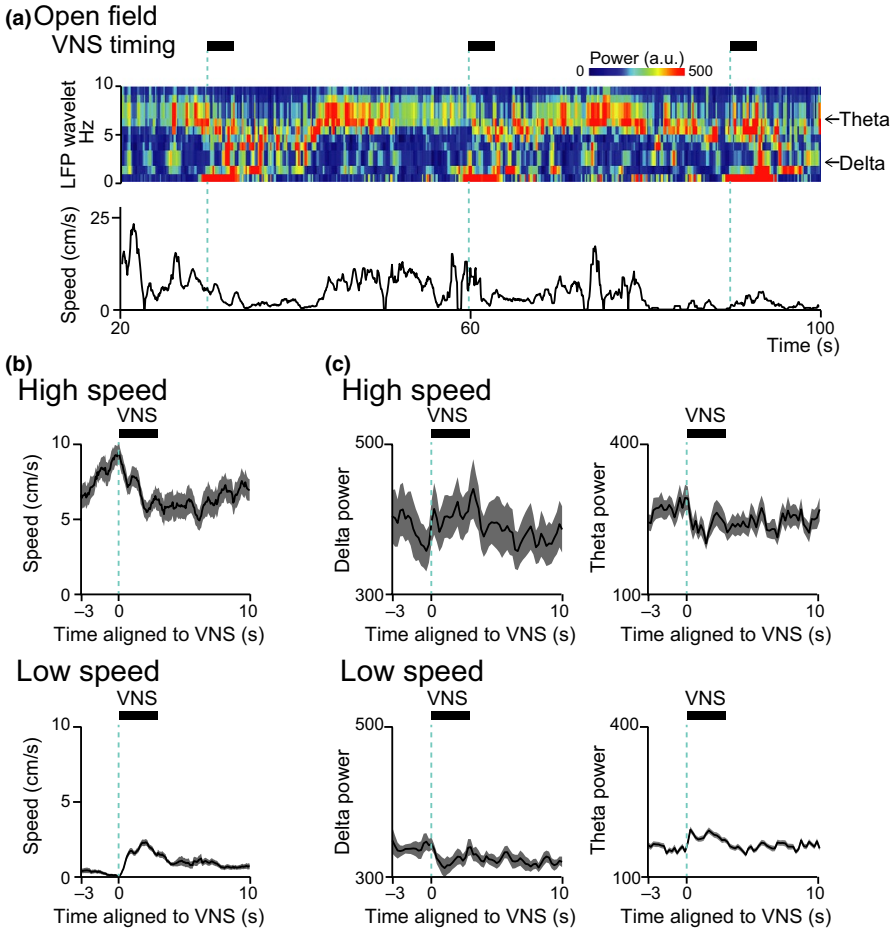

FIGURE 7 Applying VNS alters running speed and cortical activity states. (a) (From top to bottom) A color-coded power spectrum of a cortical LFP trace (blue, lower power; red higher power) and the corresponding animal's running speed in response to VNS (black horizontal bars above). (b) Changes in running speed aligned to the timing of VNS applied at high (top) and low (bottom) running speeds. The black line represents average and the shaded gray area represents mean ± SEM. The black horizontal bars above indicate the timing of VNS ($n = 5$ animals). High speed: $t_{36} = 2.35$, $p = 0.025$; low speed: $t_{102} = 10.12$, $p = 4.3 \times 10^{-17}$, paired t test, 3-s periods before vs. during VNS. *B,* Same as in *B* but for changes in delta and theta power evoked by VNS at high (top) and low (bottom) running speeds. High speed, delta: $t_{77} = 2.14$, $p = 0.035$; low speed, delta: $t_{201} = 2.92$, $p = 0.0040$; High speed, theta: $t_{77} = 5.27$, $p = 1.2 \times 10^{-6}$; low speed, theta: $t_{201} = 6.23$, $p = 2.7 \times 10^{-9}$, paired t test, 3-s periods before vs. during VNS. [Colour figure can be viewed at wileyonlinelibrary.com]

induced the opposite effects (delta: $t_{201} = 2.92$, $p = 0.0040$; theta: $t_{201} = 6.23$, $p = 2.7 \times 10^{-9}$). Taken together, these results suggest that a transient increase in VN activity evoked by VNS has the potential to acutely alter running speed and cortical arousal levels, which are bi-directional effects depending on the animal's behavioral patterns.

4 | DISCUSSION

Unveiling spike patterns of the vagus nerve is indispensable to further understand the communication between the brain and visceral organs such as the heart (Hayakawa et al., 2011), digestive organs (Campos et al., 2012; Czaja et al., 2006), and the lung (Han et al., 2018; Weijs et al., 2015). In previous studies, recordings of VN spikes have been performed in anesthetized rodent animals (Caravaca et al., 2017; Harreby et al., 2011; McCallum et al., 2017; Silverman et al., 2018). Here, we developed a new method to record electrical spikes from the cervical VN using a cuff-shaped electrode in a freely moving animal, which was integrated with our existing method to record bioelectrical signals from multiple organs, including the brain, cardiac system, breathing system, and skeletal muscle. Electrical signals arising from the VN were apparently distinct from any other central or peripheral signals. We must note that our method could not dissociate between afferent and efferent fibers enclosed in the bundle of the VN. Given that both fiber types have homogeneous spike probabilities and frequencies, the majority of the detected spike signals would arise from the afferent fibers based on the anatomical evidence that more than 80% of VN fibers transmit afferent

signals (Agostoni et al., 1957; Evans & Murray, 1954; Prechtl & Powley, 1990).

Rodent animals have a habit of changing behavioral patterns in response to the novelty of external contexts. By utilizing the behavioral characteristics, diverse animal behavioral patterns were induced, ranging from completely immobile behavior to active exploratory behavior, by placing animals into different environments, a familiar rest box and a novel open field. Our analysis confirmed that instantaneous VN spike rates were partly correlated with the animal's running speed, but the correlation was weaker than the correlation between running speed and heart rates. This lack of a perfect correlation is explained by the observations that VN spikes were increased even during active stop periods (Figure 5b), and there was a delay in the VN spike reductions relative to running speed decreases (Figure 6c).

Based on running speed, BR ratio, EMG amplitude, and heart rates, all recording periods were classified into four peripheral activity states, which were ranked from active to inactive states: movement, sniffing, active stop, and silent stop. According to this order of peripheral states, increases/decreases in cortical LFP delta/theta power, a factor used to estimate an animal's arousal and movement levels, progressed in the novel field. On the other hand, changes in the patterns of VN spike rates were not precisely aligned to this order. VN spike rates were highest during the movement periods and lowest during silent stop periods, which is consistent with changes in cortical LFP delta/theta power. However, VN spike rates during sniffing and active stop periods differed from what could be expected based on the activity level order. Interestingly, VN spike rates were transiently reduced during sniffing, a behavioral sign of attention and exploration. A possible explanation for this result might be that sniffing behavior arises from an internal state specifically processed by the central nervous system and is independent of peripheral organs. During active stop periods, in which animals stopped but their peripheral activity remained at high activity levels, VN spike rates differed between the rest box and open field, meaning that the animals were dependent on external contexts even when they exhibited similar levels of locomotion and peripheral activity. The results suggest that VN spikes during active stop periods may represent changes in internal processing of the brain–body signals in response to external environments.

The functional significance of the increased VN spikes lasting for a few seconds after reaching maximum running speed (Figure 6) remains to be understood. A possible explanation might be that increased locomotor activity activates visceral organs such as the heart, digestive organs, and the respiratory system, through increased blood flow or sympathetic tone, which in turn leads to the persistent activation of the afferent VN pathways including the heart–brain axis, gut–brain axis, and lung–brain axis.

We found that the application of VNS reduced motor behavior and cortical theta power at high-speed running, whereas it induced reverse effects at low-speed running. These results suggest that VNS has a potential to bi-directionally adjust locomotor behavior and cortical arousal states to a moderate level, avoiding extremely low or high levels. While the exact mechanisms and functional relevance remain to be elucidated, a possible mechanism of VNS to reduce locomotion during high-speed running might be through the activation of the efferent parasympathetic pathway (Yamakawa et al., 2015). On the other hand, a possible mechanism of VNS to increase locomotion and arousal states during low-speed stopping might be through the activation of multiple cortical regions (Alexander et al., 2017; Cao et al., 2016; Larsen et al., 2016; Usami et al., 2013), which might also underlie amelioration effects for treatment-resistant depression (Nemeroff et al., 2006; Wani et al., 2013).

Our study uncovered physiological spike patterns of the VNs in freely moving animals. The findings of the present study indicate that the VN has unique spike characteristics that are neither precisely correlated with brain activity nor accounted for simply by the dynamics of single peripheral organs. Further studies with more data sample collections from a variety of behavioral environments and physiological techniques to manipulate temporal dynamics of VN (e.g., Han et al., 2018) are required to reveal the functional roles of the VN in various behavioral patterns.

ACKNOWLEDGEMENTS

This work was supported by Kaken-hi (17H05939; 17H05551), a grant-in-aid for Precursory Research for Embryonic Science and Technology from the Japan Science and Technology Agency, the Exploratory Research for Advanced Technology, the Nakatomi Foundation, the Suzuken Memorial Foundation, and the Yamada Research Grant.

CONFLICT OF INTEREST

The authors declare that they have no conflict of interest.

DATA ACCESSIBILITY

The data are available from the authors.

AUTHORS' CONTRIBUTION

Y.S., T.O., and T.S. designed the work. Y.S., Y.N., and T.O. performed surgery and set experimental apparatus. T.O. acquired electrophysiological data. Y.S. and T.S. performed analysis. Y.I. supervised the project. T.S. prepared all figures and wrote the main manuscript text. All authors reviewed the main manuscript text.

ORCID

Yuji Ikegaya https://orcid.org/0000-0003-2260-8191
Takuya Sasaki https://orcid.org/0000-0001-8446-1952

REFERENCES

Agostoni, E., Chinnock, J. E., De Daly, M. B., & Murray, J. G. (1957). Functional and histological studies of the vagus nerve and its branches to the heart, lungs and abdominal viscera in the cat. *The Journal of Physiology*, *135*, 182–205. https://doi.org/10.1113/jphysiol.1957.sp005703

Alexander, G. M., Huang, Y., Soderblom, E. J., He, X. P., Moseley, A. M., & McNamara, J. O. (2017). Vagal nerve stimulation modifies neuronal activity and the proteome of excitatory synapses of amygdala/piriform cortex. *Journal of Neurochemistry*, *140*, 629–644. https://doi.org/10.1111/jnc.13931

Alvarez-Dieppa, A. C., Griffin, K., Cavalier, S., & McIntyre, C. K. (2016). Vagus nerve stimulation enhances extinction of conditioned fear in rats and modulates Arc protein, CaMKII, and GluN2B-Containing NMDA receptors in the basolateral amygdala. *Neural Plasticity*, *2016*, 4273280.

Ben-Menachem, E., Manon-Espaillat, R., Ristanovic, R., Wilder, B. J., Stefan, H., Mirza, W., … Wernicke, J. F. (1994). Vagus nerve stimulation for treatment of partial seizures: 1. A controlled study of effect on seizures. First International Vagus Nerve Stimulation Study Group. *Epilepsia*, *35*, 616–626. https://doi.org/10.1111/j.1528-1157.1994.tb02482.x

Buzsaki, G. (2006). *Rhythms of the brain*. New York, NY: Oxford University Press. https://doi.org/10.1093/acprof:oso/9780195301069.001.0001

Campos, C. A., Wright, J. S., Czaja, K., & Ritter, R. C. (2012). CCK-induced reduction of food intake and hindbrain MAPK signaling are mediated by NMDA receptor activation. *Endocrinology*, *153*, 2633–2646. https://doi.org/10.1210/en.2012-1025

Cao, B., Wang, J., Shahed, M., Jelfs, B., Chan, R. H. M., & Li, Y. (2016). Vagus nerve stimulation alters phase synchrony of the anterior cingulate cortex and facilitates decision making in rats. *Scientific Reports*, *6*, 35135. https://doi.org/10.1038/srep35135

Caravaca, A. S., Tsaava, T., Goldman, L., Silverman, H., Riggott, G., Chavan, S. S., … Olofsson, P. S. (2017). A novel flexible cuff-like microelectrode for dual purpose, acute and chronic electrical interfacing with the mouse cervical vagus nerve. *Journal of Neural Engineering*, *14*, 066005. https://doi.org/10.1088/1741-2552/aa7a42

Czaja, K., Ritter, R. C., & Burns, G. A. (2006). Vagal afferent neurons projecting to the stomach and small intestine exhibit multiple N-methyl-D-aspartate receptor subunit phenotypes. *Brain Research*, *1119*, 86–93. https://doi.org/10.1016/j.brainres.2006.08.042

Evans, D. H., & Murray, J. G. (1954). Histological and functional studies on the fibre composition of the vagus nerve of the rabbit. *Journal of Anatomy*, *88*, 320–337.

Garfinkel, S. N., & Critchley, H. D. (2016). Threat and the body: How the heart supports fear processing. *Trends in Cognitive Sciences*, *20*, 34–46. https://doi.org/10.1016/j.tics.2015.10.005

Han, W., Tellez, L. A., Perkins, M. H., Perez, I. O., Qu, T., Ferreira, J., … de Araujo, I. E. (2018). A neural circuit for gut-induced reward. *Cell*, *175*, 887–888. https://doi.org/10.1016/j.cell.2018.10.018

Harreby, K. R., Sevcencu, C., & Struijk, J. J. (2011). Early seizure detection in rats based on vagus nerve activity. *Medical and Biological Engineering and Computing*, *49*, 143–151. https://doi.org/10.1007/s11517-010-0683-1

Hayakawa, T., Kuwahara-Otani, S., Maeda, S., Tanaka, K., & Seki, M. (2011). Projections of calcitonin gene-related peptide immunoreactive neurons in the vagal ganglia of the rat. *Journal of Chemical Neuroanatomy*, *41*, 55–62. https://doi.org/10.1016/j.jchemneu.2010.11.003

Hayashi, Y., Kashiwagi, M., Yasuda, K., Ando, R., Kanuka, M., Sakai, K., & Itohara, S. (2015). Cells of a common developmental origin regulate REM/non-REM sleep and wakefulness in mice. *Science*, *350*, 957–961. https://doi.org/10.1126/science.aad1023

Johannessen, H., Revesz, D., Kodama, Y., Cassie, N., Skibicka, K. P., Barrett, P., … Chen, D. (2017). Vagal blocking for obesity control: A possible mechanism-of-action. *Obesity Surgery*, *27*, 177–185. https://doi.org/10.1007/s11695-016-2278-x

Larsen, L., Wadman, W., van Mierlo, P., Delbeke, J., Grimonprez, A., Nieuwenhuyse, B., … Raedt, R. (2016). Modulation of hippocampal activity by vagus nerve stimulation in freely moving rats. *Brain Stimulation*, *9*, 124–132. https://doi.org/10.1016/j.brs.2015.09.009

McCallum, G. A., Sui, X., Qiu, C., Marmerstein, J., Zheng, Y., Eggers, T. E., … Durand, D. M. (2017). Chronic interfacing with the autonomic nervous system using carbon nanotube (CNT) yarn electrodes. *Scientific Reports*, *7*, 11723. https://doi.org/10.1038/s41598-017-10639-w

Nemeroff, C. B., Mayberg, H. S., Krahl, S. E., McNamara, J., Frazer, A., Henry, T. R., … Brannan, S. K. (2006). VNS therapy in treatment-resistant depression: Clinical evidence and putative neurobiological mechanisms. *Neuropsychopharmacology*, *31*, 1345–1355. https://doi.org/10.1038/sj.npp.1301082

Oishi, Y., Takata, Y., Taguchi, Y., Kohtoh, S., Urade, Y., & Lazarus, M. (2016). Polygraphic recording procedure for measuring sleep in mice. *Journal of Visualized Experiments*, *107*, e53678. https://doi.org/10.3791/53678

Okada, S., Igata, H., Sakaguchi, T., Sasaki, T., & Ikegaya, Y. (2016). A new device for the simultaneous recording of cerebral, cardiac, and muscular electrical activity in freely moving rodents. *Journal of Pharmacological Sciences*, *132*, 105–108. https://doi.org/10.1016/j.jphs.2016.06.001

Okonogi, T., Nakayama, R., Sasaki, T., & Ikegaya, Y. (2018). Characterization of peripheral activity states and cortical local field potentials of mice in an elevated plus maze test. *Frontiers in Behavioral Neuroscience*, *12*, 62. https://doi.org/10.3389/fnbeh.2018.00062

Pena, D. F., Childs, J. E., Willett, S., Vital, A., McIntyre, C. K., & Kroener, S. (2014). Vagus nerve stimulation enhances extinction of conditioned fear and modulates plasticity in the pathway from the ventromedial prefrontal cortex to the amygdala. *Frontiers in Behavioral Neuroscience*, *8*, 327.

Pfeifer, G., Garfinkel, S. N., van Praag, C. D., Sahota, K., Betka, S., & Critchley, H. D. (2017). Feedback from the heart: Emotional learning and memory is controlled by cardiac cycle, interoceptive accuracy and personality. *Biological Psychology*, *126*, 19–29. https://doi.org/10.1016/j.biopsycho.2017.04.001

Prechtl, J. C., & Powley, T. L. (1990). The fiber composition of the abdominal vagus of the rat. *Anatomy and Embryology*, *181*, 101–115.

Sahin, M., & Durand, D. M. (1998). Improved nerve cuff electrode recordings with subthreshold anodic currents. *IEEE Transactions*

on Bio-Medical Engineering, *45*, 1044–1050. https://doi.org/10.1109/10.704873

Sasaki, T., Nishimura, Y., & Ikegaya, Y. (2017). Simultaneous recordings of central and peripheral bioelectrical signals in a freely moving rodent. *Biological and Pharmaceutical Bulletin*, *40*, 711–715. https://doi.org/10.1248/bpb.b17-00070

Shikano, Y., Ikegaya, Y., & Sasaki, T. (2018). Monitoring brain neuronal activity with manipulation of cardiac events in a freely moving rat. *Neuroscience Research*, *136*, 56–62. https://doi.org/10.1016/j.neures.2018.02.004

Shikano, Y., Sasaki, T., & Ikegaya, Y. (2018). Simultaneous recordings of cortical local field potentials, electrocardiogram, electromyogram, and breathing rhythm from a freely moving rat. *Journal of Visualized Experiments*, *134*, e56980. https://doi.org/10.3791/56980

Silverman, H. A., Stiegler, A., Tsaava, T., Newman, J., Steinberg, B. E., Battinelli Masi, E., … Tracey, K. J. (2018). Standardization of methods to record Vagus nerve activity in mice. *Bioelectronic Medicine*, *4*, 3. https://doi.org/10.1186/s42234-018-0002-y

Suarez, A. N., Hsu, T. M., Liu, C. M., Noble, E. E., Cortella, A. M., Nakamoto, E. M., … Kanoski, S. E. (2018). Gut vagal sensory signaling regulates hippocampus function through multi-order pathways. *Nature Communications*, *9*, 2181. https://doi.org/10.1038/s41467-018-04639-1

Takaya, M., Terry, W. J., & Naritoku, D. K. (1996). Vagus nerve stimulation induces a sustained anticonvulsant effect. *Epilepsia*, *37*, 1111–1116. https://doi.org/10.1111/j.1528-1157.1996.tb01033.x

Usami, K., Kano, R., Kawai, K., Noda, T., Ishiramatsu, T., Saito, N., & Takahashi, H. (2013). Modulation of cortical synchrony by vagus nerve stimulation in adult rats. *2013 35th Annual International Conference of the IEEE Engineering in Medicine and Biology Society (EMBC)*, *1*, 5348–5351.

Wani, A., Trevino, K., Marnell, P., & Husain, M. M. (2013). Advances in brain stimulation for depression. *Annals of Clinical Psychiatry*, *25*, 217–224.

Weijs, T. J., Ruurda, J. P., Luyer, M. D., Nieuwenhuijzen, G. A., van Hillegersberg, R., & Bleys, R. L. (2015). Topography and extent of pulmonary vagus nerve supply with respect to transthoracic oesophagectomy. *Journal of Anatomy*, *227*, 431–439. https://doi.org/10.1111/joa.12366

Woodbury, D. M., & Woodbury, J. W. (1990). Effects of vagal stimulation on experimentally induced seizures in rats. *Epilepsia*, *31*(Suppl. 2), S7–S19. https://doi.org/10.1111/j.1528-1157.1990.tb05852.x

Yamakawa, K., Rajendran, P. S., Takamiya, T., Yagishita, D., So, E. L., Mahajan, A., … Vaseghi, M. (2015). Vagal nerve stimulation activates vagal afferent fibers that reduce cardiac efferent parasympathetic effects. *American Journal of Physiology Heart and Circulatory Physiology*, *309*, H1579–H1590. https://doi.org/10.1152/ajpheart.00558.2015

How to cite this article: Shikano Y, Nishimura Y, Okonogi T, Ikegaya Y, Sasaki T. Vagus nerve spiking activity associated with locomotion and cortical arousal states in a freely moving rat. *Eur J Neurosci*. 2019;49:1298–1312. https://doi.org/10.1111/ejn.14275